BSO Crystals for the HHCAL Detector Concept

Fan Yang[1], Hui Yuan[2], Liyuan Zhang[1] and Ren-Yuan Zhu[1]
[1] 256-48, HEP, California Institute of Technology, Pasadena, CA 91125, USA
[2] Shanghai Institute of Ceramics, Shanghai, 264000, PRC

E-mail: zhu@hep.caltech.edu

Abstract. We report an investigation on optical and scintillation properties and radiation hardness of four 20 cm long BSO crystals grown at SIC for the HHCAL detector concept. Their optical and scintillation properties, such as longitudinal transmittance, light output and light response uniformity, were measured before and after γ-ray irradiation. Progresses are observed in optical quality, light output and radiation hardness. Their use for HHCAL concept is discussed.

1. Introduction

Aiming at the best jet-mass resolution cost-effective inorganic crystal scintillators are being developed for a homogeneous hadronic calorimeter (HHCAL) detector concept with dual readout of both Cherenkov and scintillation light for future high energy lepton colliders [1]. Figure 1 shows a schematic of a typical HHCAL cell with a pointing geometry with dual readout [2]. Because of the unprecedented volume (70 to 100 m^3) foreseen for the HHCAL detector concept cost-effectiveness is the most important requirement. In addition, the material must be dense to reduce the calorimeter volume, UV transparent for effective collection of the Cherenkov light, and allow for a clear discrimination between the Cherenkov and scintillation light. The preferred scintillation light is thus at a longer wavelength, and not necessarily bright nor fast. Inorganic crystals being investigated are lead fluoride (PbF_2) [2,3], lead chloride fluoride (PbFCl) [4-6] and bismuth silicate ($Bi_4Si_3O_{12}$ or BSO) [7-9]. Because of its low UV cut-off wavelength (300 nm) and low raw material cost (<50% of BGO), BSO crystals are under development at Shanghai Institute of Ceramics (SIC).

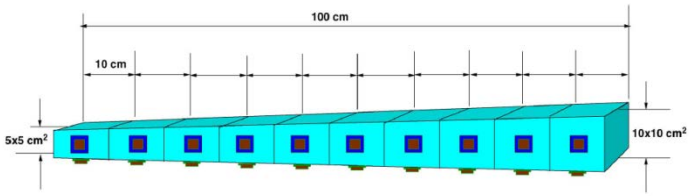

Figure 1. A schematic showing a typical cell for the HHCAL detector concept

Figure 2. Four 20 cm long BSO crystal samples grown at SIC

Figure 2 shows four BSO crystal samples grown at SIC by modified Bridgman method. Samples 12-2211 and 12-2223 were grown in 2012. Samples 13-05 and 13-09 were grown in 2013. While samples 12-2223, 13-05 and 13-09 are of a dimension of 20×20×200 mm^3, sample SIC 12-2211 is 15×15×200 mm^3. Their longitudinal transmittance (LT) was measured by using a PerkinElmer LAMBDA 950 UV/Vis spectrophotometer. The systematic uncertainty in repeated measurements is about 0.15%. Their scintillation light output (LO) was measured before and after irradiation by using a Hamamatsu R2059 PMT with a bi-alkali photo-cathode and a quartz window. For the light output measurement, one end of the samples was coupled to the PMT with Dow Corning 200 fluid while all other faces of the sample were wrapped with Tyvek paper. A collimated ^{137}Cs source was used to excite the crystals. The γ-ray peak positions were obtained by a simple Gaussian fit, and were used to determine photoelectron numbers by using calibrations of the single photoelectron peak.

2. Initial optical and scintillation properties

Figure 3 shows initial LT spectra before irradiation together with the emission spectrum for all samples. Also shown in the figure is the numerical values of the emission weighted longitudinal transmittance (EWLT), which is defined as [10]:

$$EWLT = \frac{\int LT(\lambda)Em(\lambda)d\lambda}{\int Em(\lambda)d\lambda} \qquad (1)$$

EWLT represents crystal's transparency better than the transmittance at the emission peak since it runs through the entire emission spectrum. Two observations are in order: (1) the longitudinal transmittance between 500 to 800 nm of the sample SIC 12-2211 approaches the theoretical limit, which was calculated assuming multiple bouncing without internal absorption [11]; and (2) the amplitudes of the permanent absorption bands observed between 300 and 500 nm are significantly reduced in the sample SIC 13-09 as compared to all other samples. These observations indicate that the optical quality of BSO crystals may be further improved.

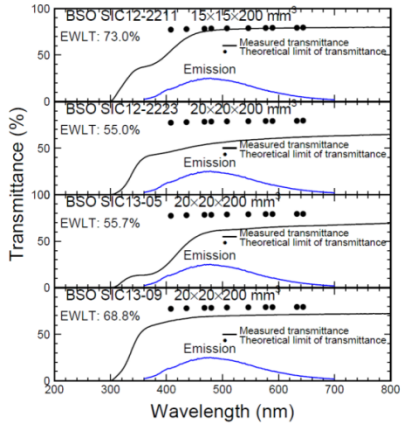

Figure 3. Initial LT of four BSO samples

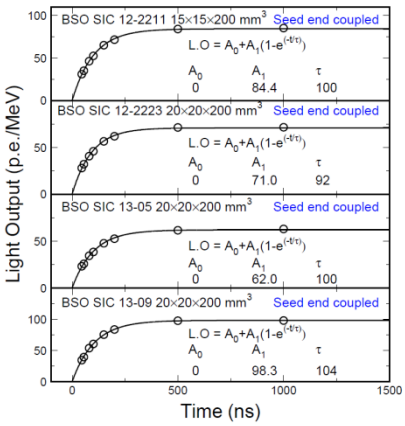

Figure 4. Initial Decay kinetics of four BSO samples

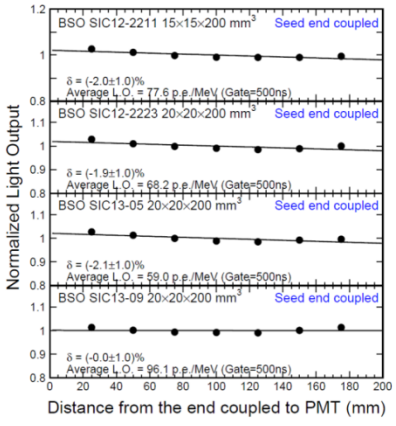

Figure 5. Initial LO and LRU of four BSO samples

Figure 4 shows the initial decay kinetics measured before irradiation for all samples. The scintillation decay time is about 100 ns. Figure 5 shows the initial light output (LO) and light response uniformity (LRU) measured before irradiation for all samples. The light response uniformity of long crystals was measured by moving a collimated γ-ray source along the longitudinal axis of the crystal at seven points evenly distributed along the crystal. The corresponding response (y) was fitted to a linear function [12]:

$$\frac{y}{y_{mid}} = 1 + \delta\left(\frac{x}{x_{mid}} - 1\right), \qquad (2)$$

where y_{mid} represents the light output at the middle of the crystal, δ represents the light response non-uniformity and x is the distance from one end of the crystal. Figure 5 shows that the non-uniformity

observed in all samples are almost flat, and the sample SIC 13-09 has the best LO and LRU because of its best optical quality among all four samples.

3. Gamma ray induced radiation damage

Radiation damage in samples SIC 12-2211, 13-05 and 13-09 was found recover under room temperature, so they were irradiated by γ-rays at 2, 8, and 30 rad/h step by step until reaching equilibrium. Radiation damage in sample SIC 12-2223 does not recover under room temperature, so it was irradiated with integrated doses from 100 to 1 Mrad stepwise increased in an order of magnitude. The main consequence of γ-ray induced radiation damage in BSO crystals is radiation induced absorption which causes degradation of transmittance and light output. It may also affect crystal's light response uniformity and cause an unrecoverable degradation in the energy resolution if the light attenuation length is reduced significantly [13, 14].

3.1 γ-ray induced dose rate dependent damage in three BSO samples

Because of the recovery, the γ-ray induced radiation damage in samples 12-2211, 13-05 and 13-09 is dose rate dependent [14]. The optical transmittance and light output decreases when samples exposed to a certain dose rate until reaching equilibrium. At the equilibrium the speed of the color center formation (damage) equals to the speed of the color center annihilation (recovery), so that the color center density (radiation induced absorption) does not change unless the applied dose rate changes.

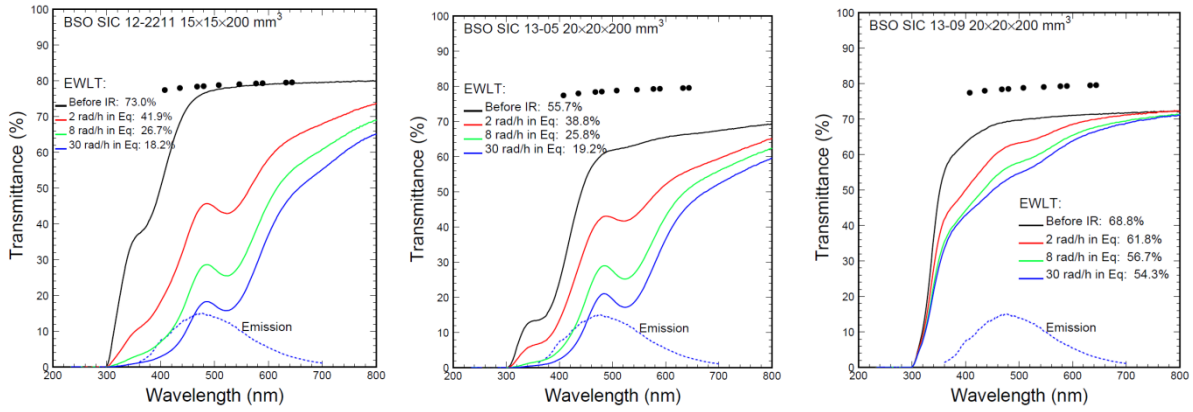

a b c

Figure 6. LT of three BSO samples in equilibrium under dose rates of 2, 8 and 30 rad/h:
a. SIC 12-2211; b. SIC 13-05; and c. SIC 13-09.

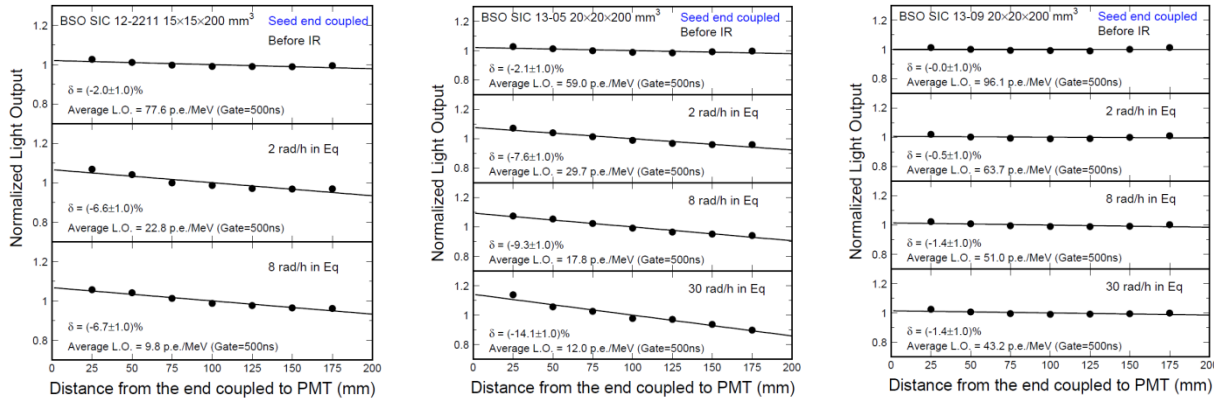

a b c

Figure 7. LO and LRU of three BSO samples in equilibrium under dose rate of 2, 8 and 30 rad/h:
a. SIC 12-2211; b. SIC 13-05; and c. SIC 13-09.

Figure 6 and 7 show LT and LO/LRU respectively of three BSO samples SIC 12-2211, 13-05 and 13-09 in equilibrium under dose rates of 2, 8, and 30 rad/h. The numerical values of EWLT are also listed in Figure 6, showing that the Sample SIC 13-09 has the lowest damage among three samples. The LO of sample SIC 12-2211 at 30 rad/h in equilibrium is not shown in Figure 7a since it is too low to be measured by using γ-rays. Figure 7c shows that the LRU of SIC 13-09 was not changed up to 30 rad/h, indicating sufficient long light attenuation length under this dose rate [14].

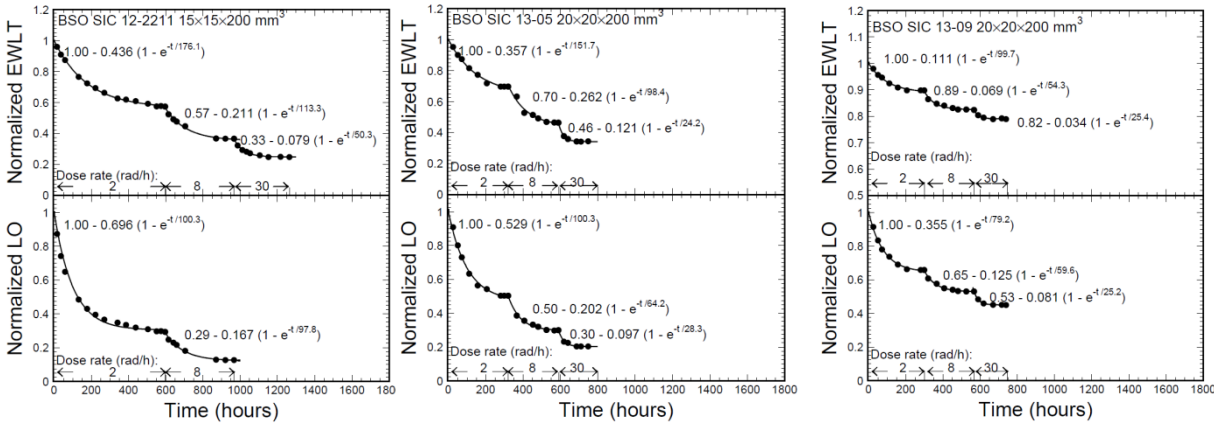

a b c

Figure 8. Histories of the normalized EWLT (top) and LO (bottom) under different dose rates: a. SIC 12-2211; b. SIC 13-05; and c. SIC 13-09.

Figure 8 shows histories of the normalized EWLT and LO for samples SIC 12-2211, 13-05 and 13-09 during γ-ray irradiations in three steps at dose rates of 2, 8 and 30 rad/h. Both EWLT and LO reached equilibrium when irradiated at a definite dose rate. The same phenomenon has also be observed in PWO [14] and BGO [15]. The damage time constants decrease when the dose rate increases, following well the color center kinetics described in [14].

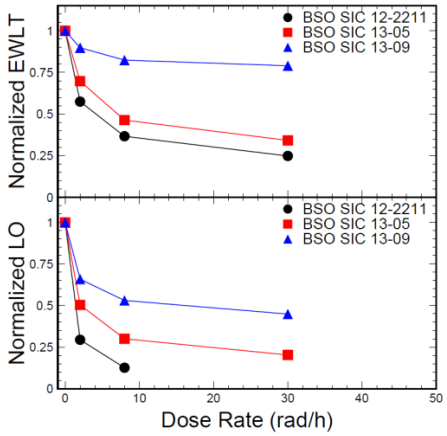

Figure 9. Normalized EWLT and LO are shown as a function of the dose rate

Table 1. EWLT and LO losses of three BSO samples in equilibrium under different dose rates

Samples		SIC 12-2211	SIC 13-05	SIC 13-09
EWLT Loss (%)	2 rad/h	43	30	10
	8 rad/h	63	54	18
	30rad/h	75	66	21
LO Loss (%)	2rad/h	71	50	34
	8rad/h	87	70	47
	30rad/h	-	80	55

Figure 9 shows the normalized EWLT (top) and LO (bottom) measured in equilibrium as a function of the dose rate for three BSO samples. The corresponding values of EWLT and LO losses are listed in table 1. It is clear that BSO samples grown in 2013 have better radiation hardness than that in 2012, and the sample SIC 13-09 has the best radiation hardness. This indicates that progress has been made in the radiation hardness of BSO crystals.

3.2 γ-ray induced dose rate independent damage in a BSO sample

Figure 10 shows that the LT of sample SIC 12-2223 does not recover after a γ-ray irradiation with a dose of 10^3 Rad. The γ-ray induced radiation damage in this sample thus is dose rate independent [14]. This sample thus was irradiated with integrated doses in steps of one order of magnitude from 10^2 to 10^6 rad. Figure 11 and 12 show LT and LO/LRU respectively for this sample at integrated doses from 10^2 to 10^6 rad. It is interesting to note that the LRU of this sample does not change although the loss of LO is significant. This indicates that energy resolution of a BSO calorimeter may be maintained up to 10^6 rad.

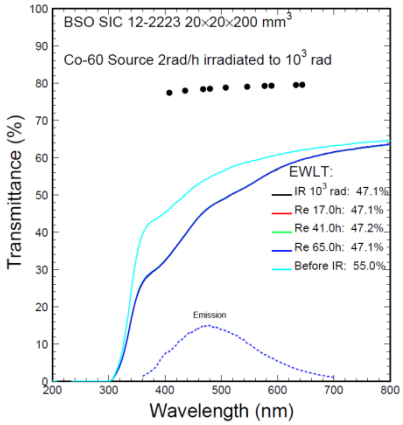

Figure 10. LT before and after irradiation of 10^3 rad for the BSO sample of SIC 12-2223.

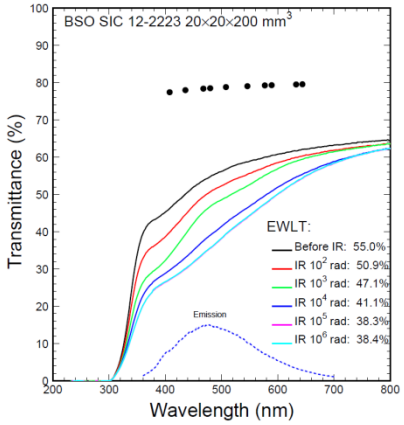

Figure 11. LT before and after irradiations of 100 to 10^6 rad is shown for sample SIC 12-2223.

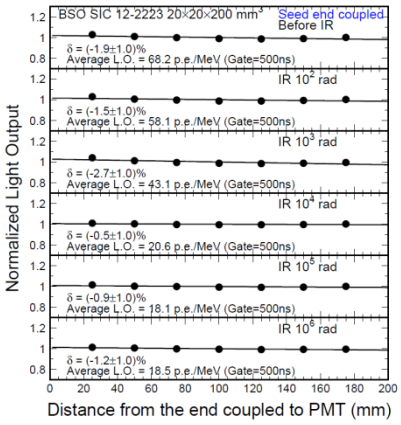

Figure 12. LO and LRU before and after irradiations are shown for sample SIC 12-2223.

Figure 13 shows the normalized EWLT and LO as a function of the integrated dose for the sample SIC 12-2223. The corresponding LO and EWLT losses after 1 Mrad are 30% and 73% respectively. The EWLT and LO losses are stable after 10^5 rad, indicating that the defect density in sample SIC 12-2223 was fully exhausted after 10^5 rad. Crystals with limited defect density have a potential to be improved for a stable detector in severe radiation environment after further reducing defect density.

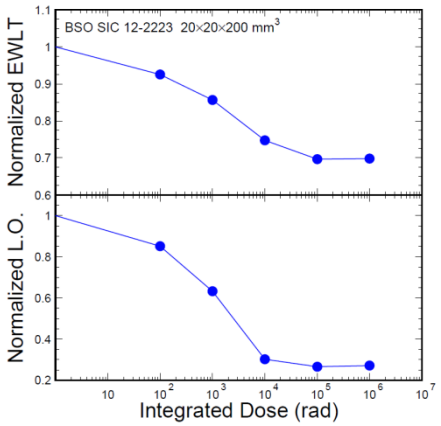

Figure 13. Normalized EWLT and LO are shown as a function of the integrated dose

Table 2. EWLT and LO losses of the BSO sample SIC 12-2223 after irradiations of different integrated dose

Integrated Dose (rad)	10^2	10^3	10^4	10^5	10^6
EWLT Loss (%)	7.5	14	25	30	30
LO Loss (%)	15	37	70	73	73

4. Summary

BSO crystals are a good candidate material for the HHCAL detector concept because of (1) high density of 6.8 g/cm3, (2) good UV cut-off edge at 300 nm, (3) emission peak at 470 nm, (4) 100 ns scintillation decay time, (5) good light output (20% of BGO) and (6) potential low cost. Among the four BSO samples grown at SIC in the last two years, SIC 12-2211 shows good transmittance approaching the theoretical limit at wavelength of longer than 500 nm, and SIC13-09 shows the improved LT, LO and LRU, indicating that progresses have been made in the crystal growth at SIC. BSO crystals satisfying HHCAL specifications, however, need to be developed after further improvement.

Gamma-ray induced radiation damage in three BSO crystals recovers at room temperature, so is dose rate dependent. The sample SIC 13-09 has better radiation hardness under gamma-ray irradiations, indicating further improvement of BSO quality is possible. Gamma-ray induced radiation damage in one BSO sample SIC 12-2223 does not recover at room temperature, so is dose rate independent. The radiation related defect density in this crystal, however, is limited, so there was no further damage after 100 kRad. Study on color centers in these crystals may help for further improvement of their radiation hardness.

Acknowledgments

This work was supported in part by the US Department of Energy Grant DE-FG03-92-ER40701 and the Natural Science Foundation of China (No. 11375250).

References

[1] Driutti A, Para A, Pauletta G, Briones N R, and Wenzel H, 2010, *J. Phys.: Conf. Ser.* (Beijing, China), **293** 012034
[2] Mao R H, Zhang L Y, and Zhu R-Y, 2012, *IEEE Trans. Nucl. Sci.*, **59**, 2229.
[3] Mao R H, Zhang L Y, and Zhu R-Y, 2010, *IEEE Trans. Nucl. Sci.*, **57**, 3841.
[4] Yang F, Zhang G Q, Ren G H, Mao R H, Zhang L Y, and Zhu R-Y, 2014, *IEEE Trans. Nucl. Sci.*, **61**, 489.
[5] Zhang G Q, Yang F, Wu Y T, Sun D D, Shang S S, and Ren G H, 2014, *J Inorg Mater*, **29**, 162.
[6] Chen J M, Shen D Z, Ren G H, Mao R H, and Yin Z W, 2004, *J Phys D Appl Phys*, **37**, 938.
[7] Fei Y T, Fan S J, Sun R Y, Xu J Y, and Ishii M, 2000, *Prog Cryst Growth Ch*, **40**, 189.
[8] Barysevich A, Dormenev V, Fedorov A, Glaser M, Kobayashi M, Korjik M, *et al.*, 2013, *Nucl Instrum Meth A*, **701**, 231.
[9] Ishii M, Harada K, Senguttuvan N, Kobayashi M, and Yamaga I, 1999, *J Cryst Growth*, **205**, 191.
[10] Chen J M, Mao R H, Zhang L Y, and Zhu R-Y, 2007, *IEEE Trans. Nucl. Sci.*, **54**, 718.
[11] Ma D A and Zhu R-Y, 1993, *Nucl Instrum Meth A*, **332**, 113.
[12] Zhu R-Y, Ma D A, Newman H B, Woody C L, Kierstead J A, Stoll S P, *et al.*, 1996, *Nucl Instrum Meth A*, **376**, 319.
[13] Zhu R-Y, 1997, *IEEE Trans. Nucl. Sci.*, **44**, 468.
[14] Zhu R-Y, 1998, *Nucl Instrum Meth A*, **413**, 297-311.
[15] Yang F, Mao R H, Zhang L Y, and Zhu R-Y, 2012, *J. Phys.: Conf. Ser.* (Santa Fe, New Mexican, USA), **404**, 012025.